Controlling the composition and magnetic properties of nano-SrFe_12 O_19 powder synthesized from oily cold mill sludge by the citrate precursor

Citation for the original published paper (version of record):
Liu, B., Zhang, S., Steenari, B. et al (2019). Controlling the composition and magnetic properties of nano-SrFe_12 O_19 powder synthesized
from oily cold mill sludge by the citrate precursor method. Materials, 12(8).
http://dx.doi.org/10.3390/ma12081250

materials

MDPI

Article

Controlling the Composition and Magnetic Properties of Nano-$SrFe_{12}O_{19}$ Powder Synthesized from Oily Cold Mill Sludge by the Citrate Precursor Method

Bo Liu [1], **Shengen Zhang** [1,*], **Britt-Marie Steenari** [2] **and Christian Ekberg** [2]

[1] Institute for Advanced Materials and Technology, University of Science and Technology Beijing, Beijing 100083, China; liubo@ustb.edu.cn
[2] Nuclear Chemistry and Industrial Material Recycling, Department of Chemistry and Chemical Engineering, Chalmers University of Technology, 41296 Gothenburg, Sweden; bms@chalmers.se (B.-M.S.); che@chalmers.se (C.E.)
* Correspondence: zhangshengen@mater.ustb.edu.cn; Tel.: +86-010-6233-3375

Received: 17 March 2019; Accepted: 12 April 2019; Published: 16 April 2019

Abstract: This paper proposes a new method for producing nano-$SrFe_{12}O_{19}$ powder by the citrate precursor route using solid waste as a source of iron. This solid iron-containing waste, which exists in the form of an oily sludge, is produced by a cold rolling mill. This sludge was first subjected to a process, including sulfuric acid leaching, oxidation, precipitation, and nitric acid leaching, to obtain an iron nitrate ($Fe(NO_3)_3$) solution. Next, the $Fe(NO_3)_3$ solution was mixed with a strontium nitrate ($Sr(NO_3)_2$) solution obtained by subjecting strontium carbonate to nitric acid leaching. Subsequently, citric acid, as chelating agent, and ammonia water, as precipitating agent, were added to the mixed solution to form a gel. The gel was dried and spontaneously combusted, then annealed at different temperatures for 2 h in flowing air. The effects of the Fe^{3+}/Sr^{2+} molar ratio and annealing temperature on the formation, morphology, and magnetic properties of $SrFe_{12}O_{19}$ were investigated. The results showed that single-phase $SrFe_{12}O_{19}$ powder was obtained by decreasing the Fe^{3+}/Sr^{2+} molar ratio from the stoichiometric value of 12 to 11.6 and increasing the annealing temperature to 1000 °C for 2 h. Adjustment of the Fe/Sr molar ratio to 12 and the annealing temperature to 900 °C enabled the magnetic properties to be optimized, including saturation magnetization (Ms) 80.2 emu/g, remanence magnetization (Mr) 39.8 emu/g, and coercive force (Hc) 6318 Oe.

Keywords: $SrFe_{12}O_{19}$; nanoparticles; citrate precursor method; industrial waste; magnetic properties

1. Introduction

The most important ferrite materials with permanent magnetic properties, M-type ferrites are widely used as magnetic recording media, microwave absorbers, magneto-optics, and other functional materials in practical applications, and they also hold promise for future use in catalysis, biology, and other fields [1–4]. Among the M-type ferrite materials, $SrFe_{12}O_{19}$ does not contain the toxic heavy metal Pb, which contributes considerably to the content of $PbFe_{12}O_{19}$. Moreover, the magnetic properties of $SrFe_{12}O_{19}$ are slightly superior to those of $BaFe_{12}O_{19}$ [5]. Therefore, $SrFe_{12}O_{19}$ has received sustained and extensive attention [6–8]. Traditionally, $SrFe_{12}O_{19}$ is prepared via a solid-state reaction process [9], which mainly involves ball milling of iron and strontium oxides, and subsequent roasting at high temperature (~1200 °C). Although this process is inexpensive and convenient, it is difficult to accurately control the chemical homogeneity, particle size distribution, and crystal defects, thereby resulting in unsatisfactory magnetic properties [10].

Attempts to overcome these problems have led to the development of non-traditional methods, such as co-precipitation [11], sol–gel [12], hydrothermal [13], molten salt-assisted [14,15], and citrate precursor [16–18]. Among these methods, the sol–gel and citrate precursor methods enable raw materials to be mixed on the ionic level and subsequent crystallization at low temperature, resulting in the production of uniform nano-$SrFe_{12}O_{19}$ [12,19]. Compared with the sol–gel method using metal alkoxide as raw material, the citrate precursor method has a relatively low production cost and simple process. Therefore, the citrate precursor method is considered to be promising for large-scale production of high-performance nano-$SrFe_{12}O_{19}$. In recent years, the preparation of nano-$SrFe_{12}O_{19}$ by the citrate precursor method has become a popular research topic. Although these studies focused on different aspects, such as process improvement [20–23] and doping modification [16,18,24], almost all of these studies utilized chemically pure nitrates as starting materials.

The rapid development of modern industry has caused the disposal of industrial solid waste to become a matter of serious global concern. In view of the wide application range and huge annual demand for $SrFe_{12}O_{19}$, the production of $SrFe_{12}O_{19}$ from industrial solid waste is not only able to realize the large-scale utilization of solid waste, but also to significantly reduce the production cost of $SrFe_{12}O_{19}$. Therefore, related studies have aroused widespread interest. Hessien et al. [25] synthesized $SrFe_{12}O_{19}$ powder with maximum saturation magnetization (Ms) 74.15 emu/g, remanence magnetization (Mr) 38.95 emu/g, and coercive force (Hc) 3455 Oe, using Egyptian celestine ore as a source of strontium, via a co-precipitation method. Xie et al. [26] reported a method for preparing $SrFe_{12}O_{19}$ powder with Ms 52.7 emu/g, Ms 29.6 emg/g, and Hc 3346 Oe from industrial strontium slag by chemical co-precipitation. Oily cold rolling mill (CRM) sludge is a metallurgical by-product produced during the process of cold rolling strip steel. In our previous research [27], $SrFe_{12}O_{19}$ powder with Ms 62.6 emu/g, Mr 32.6 emu/g, and Hc 3199 Oe was prepared by a solid phase reaction using oily CRM sludge as the source of iron. To our knowledge, preparation of nano-$SrFe_{12}O_{19}$ powder from waste by the citrate precursor method has not yet been reported.

Thus, the aim of the present paper is to report the preparation of nano-$SrFe_{12}O_{19}$ powder using oily CRM sludge as a source of iron via citrate precursor method. In addition, we also investigated the effect of annealing temperature and Fe^{3+}/Sr^{2+} molar ratio in the gel on the crystal structure, morphologies, and magnetic properties of nano-$SrFe_{12}O_{19}$ powder. The results of our study show that the proposed method presents a viable alternative for recycling industrial solid waste, and the results are helpful to understand how to control the composition and magnetic properties of nano-$SrFe_{12}O_{19}$.

2. Materials and Methods

2.1. Materials

Chemically grade sulfuric acid (H_2SO_4, 95–98%), nitric acid (HNO_3, 65–68%), strontium carbonate ($SrCO_3$, ≥97%), sodium hydroxide (NaOH, ≥96%), hydrogen peroxide solution (H_2O_2, ≥97%), citric acid ($C_6H_8O_7 \cdot H_2O$, ≥99%), and ammonia water (NH_4OH, 25–28%), were used in this study. The oily CRM sludge used in this study was obtained from a plant that manufactures cold rolled strip in China. The main components of oily CRM sludge are provided in Table 1 together with their content.

Table 1. Main composition of oily cold rolling mill (CRM) sludge.

Component	Content (wt %)
Fe	70.6
Ni	0.049
Mn	0.18
Cr	0.065
Si	0.058
V	0.024
Oil and moisture	18.2
Other	10.82

2.2. Treatment of Oily CRM Sludge

To avoid the production of toxic nitrogen oxides by direct HNO_3 leaching, the oily CRM sludge was first leached by using 6 mol/L H_2SO_4 at 85 °C for 4 h under continuous agitation. The ratio of oily CRM sludge to acid was 1:5. After leaching, filtration and centrifugation were employed to separate the acid-insoluble matter and organic compounds from the leaching solution. Then, 30 wt % H_2O_2 was added drop wise to the leaching solution until Fe^{2+} was completely oxidized to Fe^{3+}. While stirring, 5 mol/L NaOH solution, which was used as precipitant, was added to the oxidized solution until the pH reached approximately 5. As a result, ferric hydroxide ($Fe(OH)_3$) precipitated. The precipitate was removed by filtration and washed several times. Finally, solutions of ferric nitrate ($Fe(NO_3)_3$) and strontium nitrate were obtained after leaching the obtained $Fe(OH)_3$ precipitates and $SrCO_3$ by using 8 mol/L HNO_3, respectively. The above processes can be expressed as follows:

$$\mathrm{Fe\ (s) + H_2SO_4\ (aq) \rightarrow FeSO_4\ (aq) + H_2\ (g)} \tag{1}$$

$$\mathrm{Fe_2O_3\ (s) + 3H_2SO_4\ (ag) \rightarrow Fe_2(SO_4)_3\ (ag) + 3H_2O\ (L)} \tag{2}$$

$$\mathrm{FeO\ (s) + H_2SO_4\ (ag) \rightarrow FeSO_4\ (ag) + H_2O\ (L)} \tag{3}$$

$$\mathrm{2FeSO_4\ (aq) + H_2SO_4\ (aq) + H_2O_2\ (L) \rightarrow Fe_2(SO_4)_3\ (aq) + 2H_2O\ (L)} \tag{4}$$

$$\mathrm{Fe_2(SO_4)_3\ (aq) + 6NaOH\ (aq) \rightarrow 2Fe(OH)_3\ (s) + 3Na_2SO_4\ (aq)} \tag{5}$$

2.3. Preparation of Strontium Ferrites

Mixed solutions were prepared by varying the molar ratio of Fe^{3+}/Sr^{2+} from 11.6 to 12 by proportionally mixing solutions of $Fe(NO_3)_3$ and $Sr(NO_3)_2$. Then, citric acid was added to the mixed solution until the molar ratio of citric acid to the sum of Fe^{3+} and Sr^{2+} reached 1.5. Subsequently, ammonia solution (25%) was added to the mixed solution to form a solution of pH 7. A viscous gel was obtained after magnetically stirring the solution for 4 h at 60 °C. The gel was dried at 100 °C overnight, and then burned spontaneously in air. Finally, $SrFe_{12}O_{19}$ powder was obtained after the combustion product was annealed at 400–1100 °C for 2 h in flowing air. The process flow chart of $SrFe_{12}O_{19}$ powder from oily CRM sludge is shown in Figure 1.

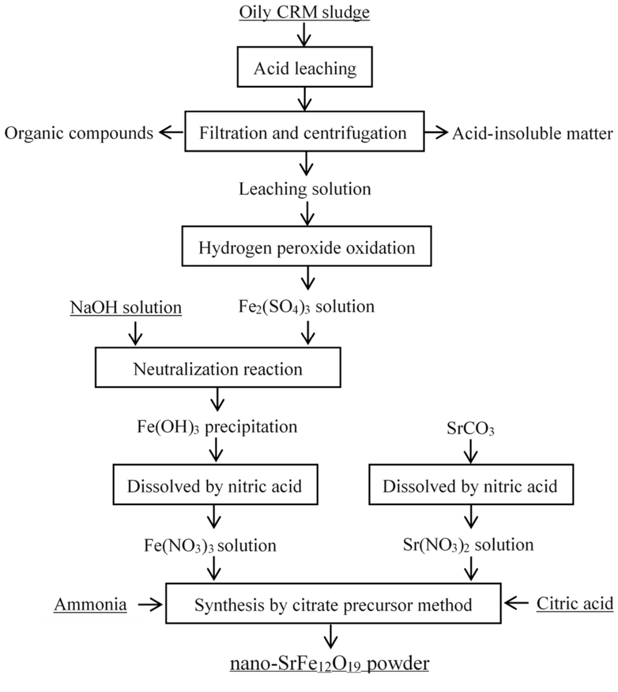

Figure 1. The process flow chart of $SrFe_{12}O_{19}$ powder obtained from oily CRM sludge.

2.4. Characterization

Inductively coupled plasma (ICP, OPTIMA 7000DV, PerkinElmer) was used to analyze the chemical composition of samples. The pH values of solutions were measured by a pH/mV meter (pHS-25, Huguang, China). The morphology of the products was observed by field-emission scanning electron microscopy (FE-SEM, Zeiss Ultra 55). Fourier transform infrared (FTIR) spectroscopy (Nicolet Nexus-470, Perkin-Elmer) was used to detect the types of functional groups present in the products. Thermogravimetric and differential scanning calorimetry (TG-DSC, STA409C, Netzsch) measurements of the samples were recorded at a heating rate of 10 °C/min in air. The magnetic properties of the obtained $SrFe_{12}O_{19}$ powder were assessed using a vibrating sample magnetometer (VSM, LDJ 9600) at room temperature. The hysteresis loops were used to determine the values of Ms, Mr, and Hc. The crystalline phases present in samples were identified by X-ray diffraction (XRD, APD-10, Philips). The mean crystallite size was determined using the Scherrer formula [28]:

$$d = K\lambda/\beta\cdot\cos\theta \tag{6}$$

where d is the mean crystallite size, K is a constant, β is the half width of the relevant diffraction reflection, λ is the X-ray wavelength, and θ is the diffraction angle. Moreover, the relative content of phases were calculated by the reference intensity ratio (RIR) method [29].

3. Results and Discussion

3.1. Effect of Annealing Temperature

The effect of the annealing temperature on the formation of $SrFe_{12}O_{19}$ was investigated by fixing the Fe^{3+}/Sr^{2+} molar ratio of the gel at the stoichiometric ratio of 12. After combustion of the dried gel, the resulting material was first analyzed by FTIR and TG-DSC, respectively. The FTIR peak (Figure 2a) at 3300 cm^{-1} is assigned to the vibration absorption of the O–H bond in citrate, which indicates the presence of citrate in the combustion products. The peaks at 1358 cm^{-1} and 1416 cm^{-1} are associated with the characteristic vibrational absorption band of NO_3^-. The broadened absorption peak near 667 cm^{-1} is the characteristic peak of γ-Fe_2O_3, which is associated with the Fe–O vibration. According to the TG-DSC analysis (Figure 2b), three distinct changes occur in the sample weight, that is, a small decrease below 280 °C, a significant decrease in the range of 280–470 °C, and stabilization above 470 °C.

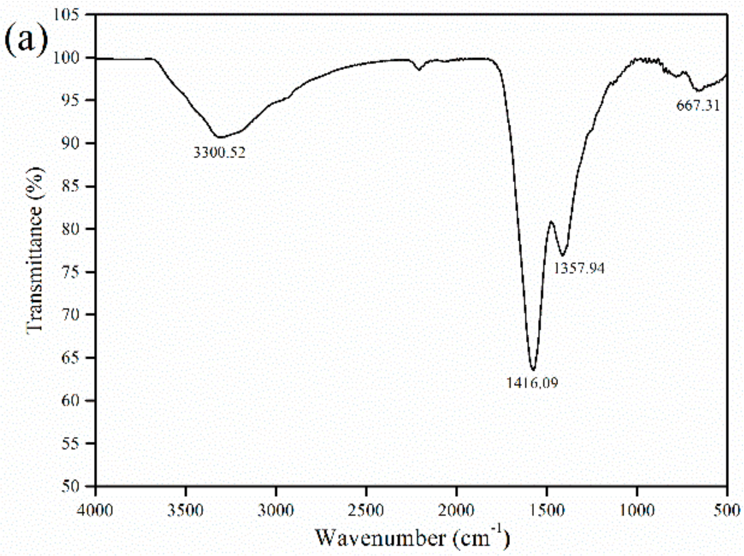

Figure 2. *Cont.*

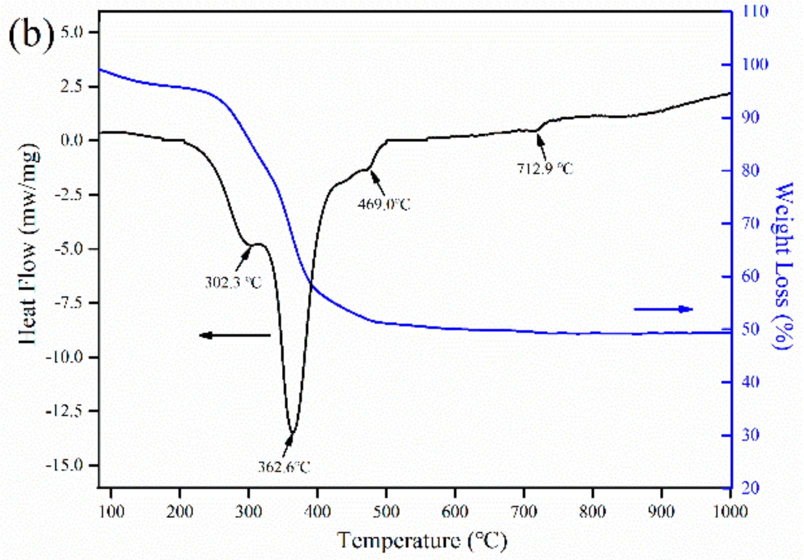

Figure 2. Analyses of the combustion products: (**a**) FTIR spectrum and (**b**) thermogravimetric and differential scanning calorimetry (TG-DSC) thermogram.

In view of the loose and porous structure of combustion products, the weight loss of the sample below 280 °C was mainly attributed to the evaporation of adsorbed moisture. Combined with the results of FTIR analysis, the significant weight loss at 280–470 °C was mainly caused by the decomposition of residual citrate, nitrate, etc. As the temperature rose above 362.6 °C, the thermal behavior of the sample changed from endothermic to exothermic. This indicates that the exothermic effect resulting from the decomposition of NH_4NO_3 (shown as equation (7)) begins to play a dominant role.

$$2NH_4NO_3 \rightarrow 2N_2\,(g) + O_2\,(g) + 4H_2O \text{ (exothermic reaction)} \quad (7)$$

To further investigate the phase changes the samples undergo during heat treatment, a series of experiments was performed by varying annealing temperature from 400 to 1100 °C. XRD patterns of untreated and heat-treated samples are shown in Figure 3a.

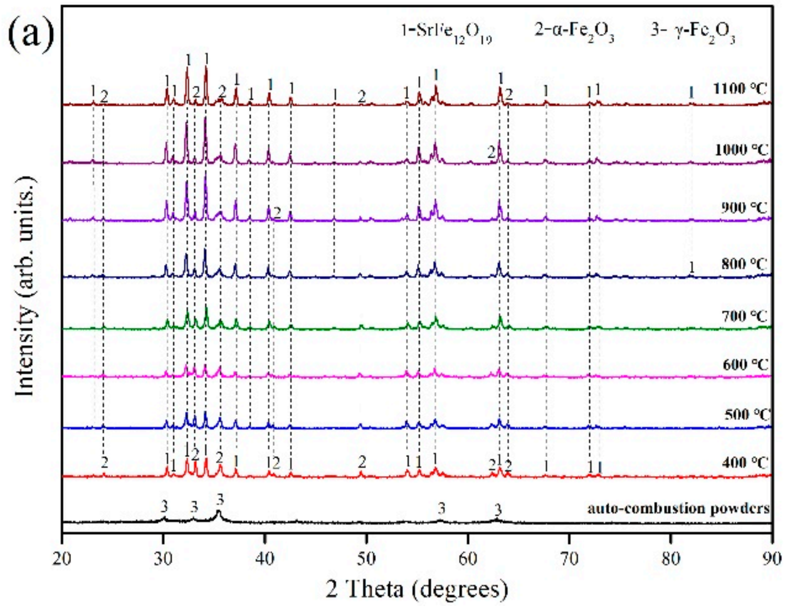

Figure 3. *Cont.*

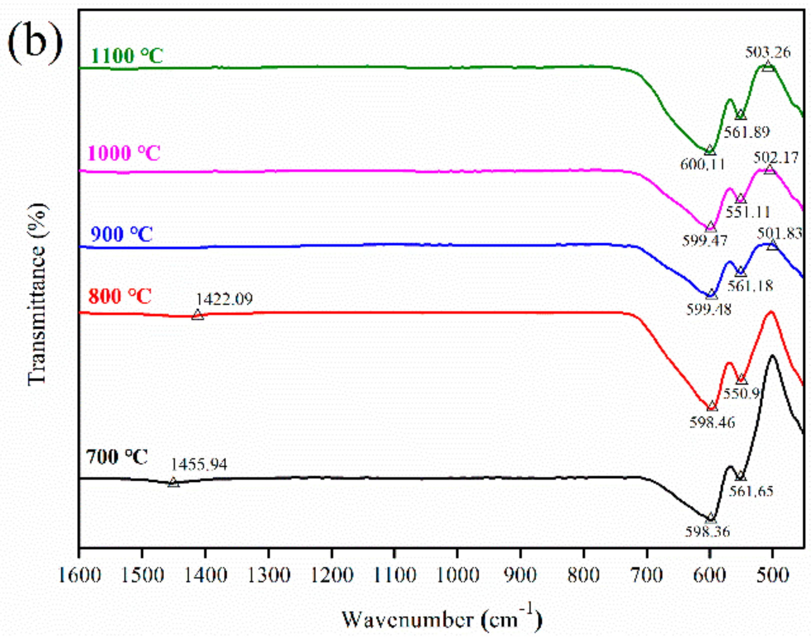

Figure 3. Analyses of untreated and heat-treated samples: (**a**) XRD patterns and (**b**) FTIR spectra.

The main crystal phase of the untreated sample was observed to be γ-Fe_2O_3, whereas the main crystalline phases of the sample annealed at 400 °C are $SrFe_{12}O_{19}$ and α-Fe_2O_3. This indicates that the following reaction occurs during the annealing process.

$$\gamma\text{-}Fe_2O_3 \rightarrow \alpha\text{-}Fe_2O_3 \quad (8)$$

The intensity and resolution of the diffraction peaks of the $SrFe_{12}O_{19}$ phase in the samples increased as the calcination temperature increased, especially above 700 °C. The increased annealing temperature significantly reduced the number and intensity of the α-Fe_2O_3 diffraction peaks in the sample. However, even at 1100 °C, a small amount of the α-Fe_2O_3 phase still existed in the sample. The samples that were obtained at various temperatures from 700 °C upward were further studied by recording their FTIR spectra (Figure 3b). The bands at 598.36 cm^{-1}, 598.46 cm^{-1}, 599.48 cm^{-1}, 599.47 cm^{-1} and 600.11 cm^{-1} correspond to the Sr–O stretching vibration band [30]. The bands at 561.65 cm^{-1}, 550.90 cm^{-1}, 561.18 cm^{-1}, 551.11 cm^{-1} and 561.89 cm^{-1} were attributed to the Fe–O stretching vibration by Fe–O_4 [31]. The bands at 501.83 cm^{-1}, 502.17 cm^{-1} and 503.26 cm^{-1} can be assigned to the Fe–O stretching vibrations of α-Fe_2O_3 [32]. This indicates the existence of $SrFe_{12}O_{19}$ and α-Fe_2O_3 in the samples, and is consistent with the results of the XRD analysis. Moreover, the samples obtained at 700 °C and 800 °C exhibited absorption peaks in the range 1400–1459 cm^{-1}, and these peaks are associated with the characteristic vibrational absorption band of NO_3^-. This indicates that a certain amount of nitrate still existed in the samples below 900 °C, and that higher temperatures were helpful to remove them. Accordingly, this explains the 0.68% weight loss detected in the TG-DSC experiment.

The SEM images of the samples obtained at different annealing temperatures (Figure 4) show that the samples obtained at 700 °C and 800 °C had poor homogeneity with extensive agglomeration, indicating that the formation of $SrFe_{12}O_{19}$ was incomplete. These results are in good agreement with those of the XRD and FTIR analyses. Above 900 °C, samples were uniform with no obvious aggregation. The particle size of the sample annealed at 900 °C were approximately 200 nm. With the increase of annealing temperature from 900 to 1000 °C, the particle size of the sample increased slightly. However, at 1100 °C, the powder particles clearly experienced abnormal growth. This may be due to the growth of particle size.

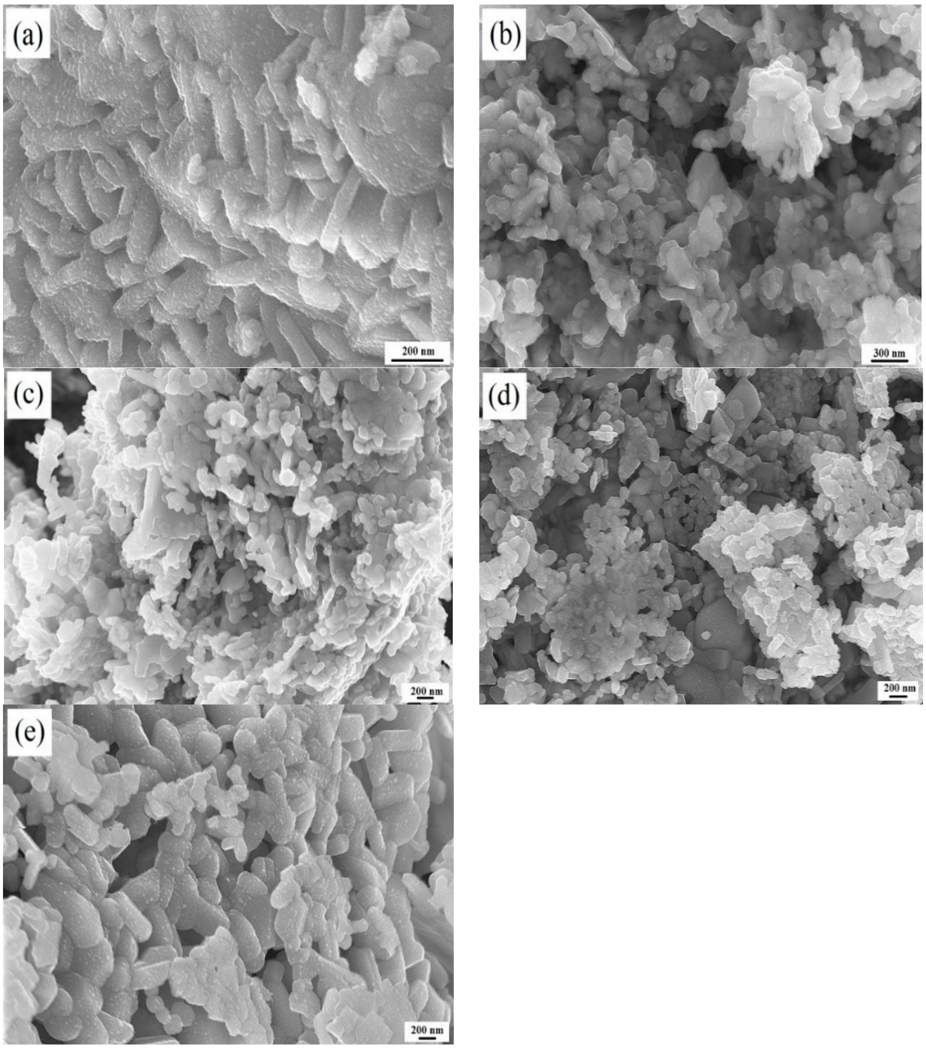

Figure 4. SEM images of products obtained at different annealing temperatures: (**a**) 700 °C; (**b**) 800 °C; (**c**) 900 °C; (**d**) 1000 °C; (**e**) 1100 °C.

The magnetic properties and crystallite size of samples as a function of temperature are summarized in Figure 5. The magnetic properties of samples increased significantly as the annealing temperature increased from 700 to 900 °C, with the highest Ms of 80.2 emu/g measured at 900 °C. Combined with the previous results, this may be ascribed to the reduction in the amount of residual nitrates, resulting in an increase in the proportion of $SrFe_{12}O_{19}$ present. Above 900 °C, the magnetic properties of the products deteriorated significantly as the annealing temperature increased. The changes in the magnetic properties can be explained by the changes in the sizes of the crystals (Figure 5b) and morphologies (Figure 4) of the samples. Excessive grain growth destroys the uniformity of samples, thus causing the deterioration of magnetic properties.

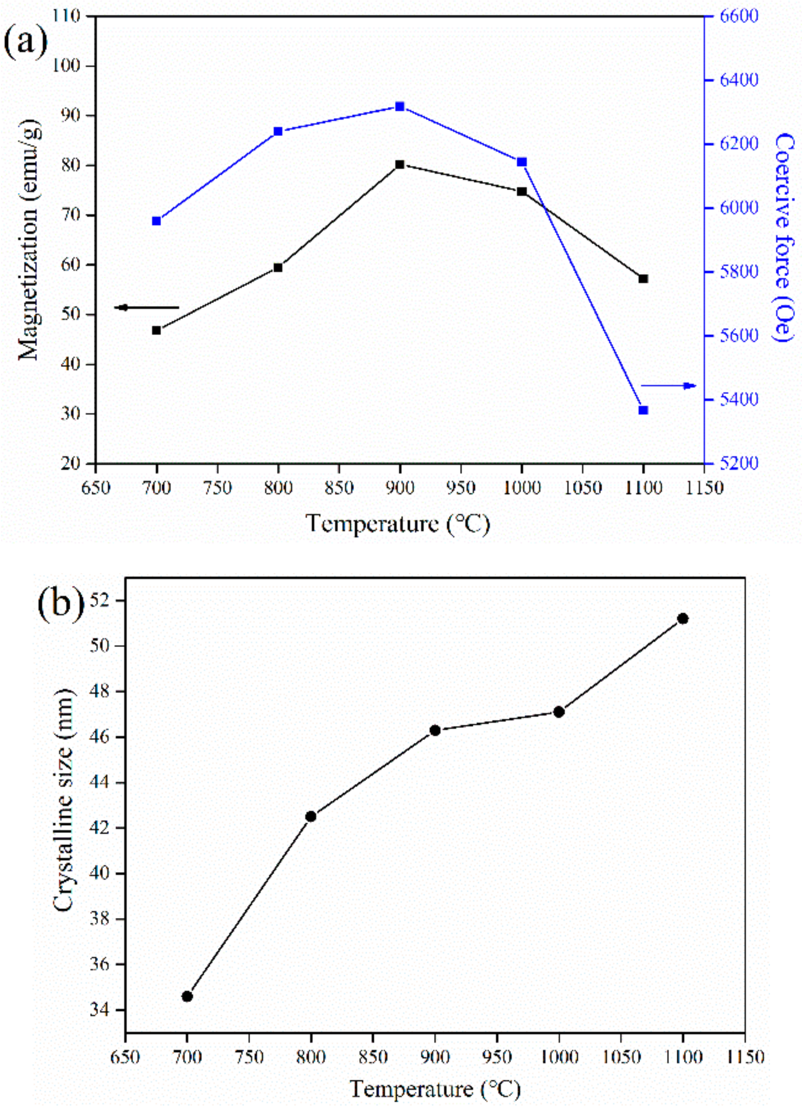

Figure 5. Effect of annealing temperature on the (**a**) magnetic properties and (**b**) crystalline size of the obtained $SrFe_{12}O_{19}$ powder.

3.2. *Effect of Fe/Sr Molar Ratio*

Previous studies have shown that an appropriate Fe/Sr molar ratio is one of the decisive factors for obtaining products with a single $SrFe_{12}O_{19}$ phase [33]. In the hydrothermal synthesis of $SrFe_{12}O_{19}$, Malick et al. [34] found that products with a single $SrFe_{12}O_{19}$ phase can be obtained at a specified Fe/Sr molar ratio. According to the studies of Hessien et al. on the preparation of $SrFe_{12}O_{19}$ via the co-precipitation method [5], the pure $SrFe_{12}O_{19}$ phase can be obtained at a Fe/Sr molar ratio of 9.23 and an annealing temperature of 900 °C. Wang et al. [35] prepared $SrFe_{12}O_{19}$ powder by using the sol–gel method, and found that the pure $SrFe_{12}O_{19}$ phase can be obtained at a Fe/Sr molar ratio of 11.5 and an annealing temperature of 800 °C.

Thus, to obtain products with a single $SrFe_{12}O_{19}$ phase, a series of experiments were performed by varying the Fe/Sr molar ratio from 11.6 to 11.8. Figure 6 shows the XRD patterns of products with an Fe/Sr molar ratio of 11.8 and annealed at different temperatures. The results of other analyses that were performed at the same time, including the phase content, crystalline size, and magnetic properties, are summarized in Table 2. These results indicate that the content of the α-Fe_2O_3 phase in the sample decreases as the annealing temperature increases. However, even at 1100 °C, it is not possible to obtain a product consisting of a single $SrFe_{12}O_{19}$ phase.

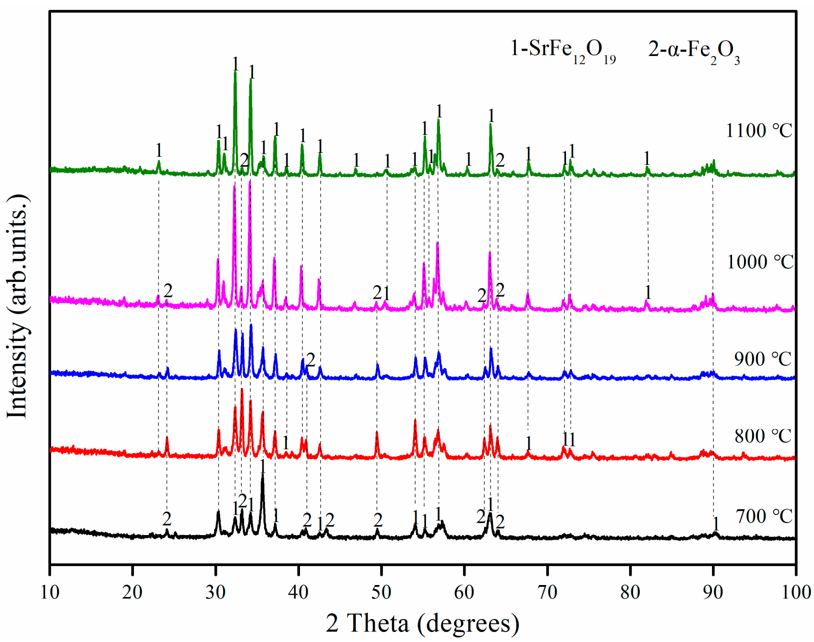

Figure 6. XRD patterns of $SrFe_{12}O_{19}$ with an Fe/Sr molar ratio of 11.8 and annealed at different temperatures.

Table 2. Effect of annealing temperature on the phase content, crystalline size, and magnetic properties of the obtained $SrFe_{12}O_{19}$ samples with an Fe/Sr molar ratio of 11.8.

Annealing Temperature (°C)	**Phase Content**	**Crystalline Size (nm)**	**Magnetic Properties**		
			Ms (emu/g)	**Mr (emu/g)**	**Hc (Oe)**
700	73% $SrFe_{12}O_{19}$ 27% α-Fe_2O_3	29.6	40.8 ± 0.1	21.3 ± 0.1	854 ± 70
800	80% $SrFe_{12}O_{19}$ 20% α-Fe_2O_3	30.2	42.7 ± 0.1	21.8 ± 0.1	4770 ± 50
900	86% $SrFe_{12}O_{19}$ 14% α-Fe_2O_3	34.6	46.9 ± 0.1	24.2 ± 0.1	5260 ± 50
1000	92% $SrFe_{12}O_{19}$ 8% α-Fe_2O_3	44.6	59.8 ± 0.1	31.1 ± 0.1	5080 ± 40

Moreover, the magnetic properties of the products listed in Table 2 increased significantly with an increase in the annealing temperature. This is mainly attributed to the increase of the $SrFe_{12}O_{19}$ phase content of the product.

Figure 7 and Table 3 present the XRD patterns of products with an Fe/Sr molar ratio of 11.4 and annealed at different temperatures. The $SrFe_{12}O_{19}$ powder samples obtained below 1000 °C contained some of the peaks associated with the α-Fe_2O_3 phase (7–15%). At 1000 °C, products with a well-crystallized single $SrFe_{12}O_{19}$ phase were obtained. Moreover, the results in Table 3 show that the magnetic properties of products increased by increasing the annealing temperature. This is attributed to an increase in the $SrFe_{12}O_{19}$ phase content in the product.

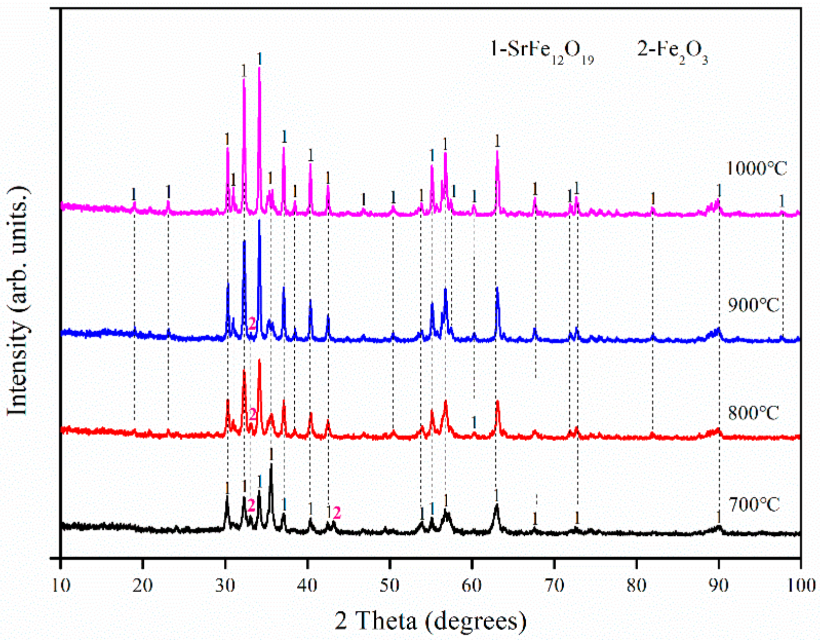

Figure 7. XRD patterns of $SrFe_{12}O_{19}$ with an Fe/Sr molar ratio of 11.6 by varying the annealing temperature.

Table 3. Effect of annealing temperature on the phase content, crystalline size, and magnetic properties of $SrFe_{12}O_{19}$ samples obtained with an Fe/Sr molar ratio of 11.6.

Annealing Temperature (°C)	Phase Content	Crystalline Size (nm)	Magnetic Properties		
			Ms (emu/g)	Mr (emu/g)	Hc (Oe)
700	85% $SrFe_{12}O_{19}$ 15% α-Fe_2O_3	45.5	45.5 ± 0.1	21.3 ± 0.1	1170.1 ± 60
800	90% $SrFe_{12}O_{19}$ 10% α-Fe_2O_3	50.1	50.1 ± 0.1	26.6 ± 0.1	5737.9 ± 30
900	93% $SrFe_{12}O_{19}$ 7% α-Fe_2O_3	58.1	58.1 ± 0.1	31.1 ± 0.1	6437.8 ± 20
1000	100% $SrFe_{12}O_{19}$	74.2	67.5 ± 0.1	36.1 ± 0.1	6176.0 ± 20

3.3. Comparison of Magnetic Properties

To summarize, two of the samples exhibited improved magnetic properties. The first is the sample with an Fe/Sr molar ratio of 12 and annealed at 900 °C, which was named $SrFe_{12}O_{19}$@900. The other is the sample with an Fe/Sr molar ratio of 11.6 and annealed at 1000 °C, which was named $SrFe_{11.6}O_{19}$@1000. These two samples were compared with those prepared from chemicals/analytical chemicals reported in the literature. The results of this comparison are presented in Table 4.

Table 4. Performance comparison between the samples obtained in this study and those reported in the literature.

Sample	Synthetic Method	Magnetic Properties		
		Ms (emu/g)	**Mr (emu/g)**	**Hc (Oe)**
$SrFe_{12}O_{19}$@900	CPM	80.2	39.8	6318
$SrFe_{11.6}O_{19}$@1000	CPM	67.5	36.1	6176
$SrFe_{12}O_{19}$ powder [20]	MA-SGM	54.8	29.5	5261
$Sr_{0.9}La_{0.1}Fe_{11.9}Co_{0.1}O_{19}$ powder [20]	SGM	73	36	7700
$Sr_{0.85}Nd_{0.15}Fe_{12}O_{19}$ powder [21]	CPM	63	35.15	6885
$SrFe_{12}O_{19}$ nanoribbons [22]	SAE	67.9	37.3	7310
$SrFe_{12}O_{19}$ powder [23]	SGM	59.3	34.9	6725

CPM = citrate precursor method; SGM = sol–gel method; MA-SGM = microwave-assisted sol–gel method; SAE = solution assisted electrospinning.

Although the content of the $SrFe_{12}O_{19}$ phase in $SrFe_{11.6}O_{19}$@1000 (100%) was higher than that in $SrFe_{12}O_{19}$@900 (97.9%), the grain size of $SrFe_{11.6}O_{19}$@1000 (74.1 nm) was significantly larger than that of $SrFe_{12}O_{19}$@900 (49.7 nm). The excessive grain growth may be the main reason why the magnetic properties of $SrFe_{11.6}O_{19}$@1000 were inferior to those of $SrFe_{12}O_{19}$@900. Moreover, Ms and Mr of $SrFe_{12}O_{19}$@900 reached 80.2 emg/g and 6318 Oe, respectively. Moreover, the comparison clearly shows that the magnetic properties of $SrFe_{12}O_{19}$@900 are competitive compared with those reported in the literature.

4. Conclusions

Using oily CRM sludge as an iron resource, nano-$SrFe_{12}O_{19}$ was synthesized successfully by using the citrate precursor method. The results showed that single-phase $SrFe_{12}O_{19}$ powder samples were obtained by decreasing the Fe/Sr molar ratio from the stoichiometric value of 12 to 11.6 and by increasing the annealing temperature to 1000 °C. An Fe/Sr molar ratio of 12 and annealing temperature of 900 °C produced nano-$SrFe_{12}O_{19}$ powder with a particle size of approximately 200 nm, and good magnetic properties (Ms 80.2 emu/g and Hc 6318 Oe), which are comparable to those of $SrFe_{12}O_{19}$ prepared from chemically pure materials.

Author Contributions: B.L. and S.Z. designed the experiments; B.L. performed the experiments, analyzed the results, and structured the manuscript; B.-M.S. and C.E. contributed with the discussions of experimental results. All authors contributed in the review of the manuscript.

Funding: This work is supported by the National Natural Science Foundation of China (Grant No. 51502014 and 51672024), the Fundamental Research Funds for the Central Universities (Grant No. FRF-TP-17-1812) and financial support from the program of China Scholarships Council (Grant No. 201806465040).

Conflicts of Interest: The authors declare no conflict of interest.

References

1. Ramezanzaeh, G.; Ghasemi, A.; Mozaffarinia, R.; Alizadeh, A. Electromagnetic wave reflection loss and magnetic properties of M-type $SrFe_{12-x}(Mn_{0.5}Sn_{0.5})_xO_{19}$ hexagonal ferrite nanoparticles in the Ku microwave band. *Ceram. Int.* **2017**, *43*, 10231–10238. [CrossRef]
2. Ashraf, G.A.; Zhang, L.T.; Abbas, W.; Murtaza, G. Synthesis and characterizations of Al-Sm substituted Ba-Sr M-type hexagonal ferrite nanoparticles via sol–gel route. *Ceram. Int.* **2018**, *44*, 18678–18685. [CrossRef]
3. Trukhanov, A.V.; Kostishyn, V.G.; Panina, L.V.; Korovushkin, V.V.; Turchenko, V.A.; Thakur, P.; Thakur, A.; Yang, Y.; Vinnik, D.A.; Yakovenko, E.S. Control of electromagnetic properties in substituted M-type hexagonal ferrites. *J. Alloys Compd.* **2018**, *754*, 247–256. [CrossRef]
4. Ueda, H.; Tanioku, Y.; Michioka, C.; Yoshimura, K. Magnetocrystalline anisotropy of La- and Co-substituted M-type strontium ferrites: Role of Co^{2+} and Fe^{2+}. *Phys. Rev. B* **2017**, *95*, 224421. [CrossRef]

5. Hessien, M.M.; Rashad, M.M.; El-Barawy, K. Controlling the composition and magnetic properties of strontium hexaferrite synthesized by co-precipitation method. *J. Magn. Magn. Mater.* **2008**, *320*, 336–343. [CrossRef]
6. Das, T.; Nicholas, J.D.; Qi, Y. Long-range charge transfer and oxygen vacancy interactions in strontium ferrite. *J. Mater. Chem. A* **2017**, *5*, 4493–4506. [CrossRef]
7. Wang, Z.H.; Zhao, L.; Wang, P.H.; Guo, L.; Yu, J.H. Low material density and high microwave-absorption performance of hollow strontium ferrite nanofibers prepared via coaxial electrospinning. *J. Alloys Compd.* **2016**, *687*, 541–547. [CrossRef]
8. Liu, C.C.; Liu, X.S.; Feng, S.J.; Rehman, K.M.U.; Li, M.L.; Zhang, C.; Li, H.H.; Meng, X.Y. Microstructure and magnetic properties of M-type strontium hexagonal ferrites with Y-Co substitution. *J. Magn. Magn. Mater.* **2017**, *436*, 126–129. [CrossRef]
9. Spaoletova, N.; Kushnir, S.; Ahn, K.; An, S.Y.; Choi, M.; Kim, J.Y.; Choi, C.; Wi, S. M-Zn (M = Sb, V, and Nb) Substituted Strontium Hexaferrites with Enhaced Saturation Magnetization for Permanent Magnet Applications. *J. Magn.* **2016**, *21*, 315–321. [CrossRef]
10. Liu, J.R.; Hong, R.Y.; Feng, W.G.; Badami, D.; Wang, Y.Q. Large-scale production of strontium ferrite by molten-salt-assisted coprecipitation. *Powder Technol.* **2014**, *262*, 142–149. [CrossRef]
11. Anis-ur-Rehman, M.; Asghar, G. Variation in structural and dielectric properties of co-precipitated nanoparticles strontium ferrites due to value of pH. *J. Alloys Compd.* **2011**, *509*, 435–439. [CrossRef]
12. Chen, X.; Wang, X.; Li, L.; Qi, S. Preparation and excellent microwave absorption properties of silver/strontium ferrite/graphite nanosheet composites via sol–gel method. *J. Mater. Sci.: Mater. Electron.* **2016**, *27*, 10045–10051. [CrossRef]
13. Xia, A.; Zuo, C.; Chen, L.; Jin, C.; Lv, Y. Hexagonal $SrFe_{12}O_{19}$ ferrites: Hydrothermal synthesis and their sintering properties. *J. Magn. Magn. Mater.* **2013**, *332*, 186–191. [CrossRef]
14. Lei, C.; Tang, S.; Du, Y. Synthesis of aligned La^{3+}-substituted Sr-ferrites via molten salt assisted sintering and their magnetic properties. *Ceram. Int.* **2016**, *42*, 15511–15516. [CrossRef]
15. Li, Y.; Bao, D.; Wang, Z.; Ye, H.; Kong, B. Synthesis of Ca^{2+} doped SrLa-ferrite powder through molten salt assisted calcination process. *J. Alloys Compd.* **2018**, *765*, 201–206.
16. Alamolhoda, S.; Mirkazemi, S.M.; Ghiami, Z.; Niyaifar, M. Structure and magnetic properties of Zr-Mn substituted strontium hexaferrite $Sr(Zr,Mn)_xFe_{12-2x}O_{19}$ nanoparticles synthesized by sol–gel auto-combustion method. *Bull. Mater. Sci.* **2016**, *39*, 1311–1318. [CrossRef]
17. Masoudpanah, S.M.; Seyyed Ebrahimi, S.A. Effect of citric acid content on the structural and magnetic properties of $SrFe_{12}O_{19}$ thin films. *Thin Solid Films* **2011**, *520*, 199–203. [CrossRef]
18. Kaur, P.; Chawla, S.K.; Meena, S.S.; Yusuf, S.M.; Bindra Narang, S. Synthesis of Co-Zr doped nanocrystalline strontium hexaferrites by sol–gel auto-combustion route using sucrose as fuel and study of their structural, magnetic and electrical properties. *Ceram. Int.* **2016**, *42*, 14475–14489. [CrossRef]
19. Thakur, A.; Singh, R.R.; Barman, P.B. Structural and magnetic properties of La^{3+} substituted strontium hexaferrite nanoparticles prepared by citrate precursor method. *J. Magn. Magn. Mater.* **2013**, *326*, 35–40. [CrossRef]
20. Brightlin, B.C.; Balamurugan, S.; Arun, T. Microstructural and magnetic features of $SrFe_{12}O_{19}$ materials synthesized from different fuels by sol–gel auto-combustion method. *J. Supercond. Novel Magn.* **2017**, *30*, 1427–1437. [CrossRef]
21. Roohani, E.; Arabi, H.; Sarhaddi, R.; Sudkhah, S.; Shabani, A. Effect of annealing temperature on structural and magnetic properties of strontium hexaferrite nanoparticles synthesized by sol–gel auto-combustion method. *Int. J. Mod. Phys. B* **2015**, *29*, 1550190. [CrossRef]
22. Chawla, S.K.; Kaur, P.; Mudsainiyan, R.K.; Meena, S.S.; Yusuf, S.M. Effect of Fuel on the Synthesis, Structural, and Magnetic Properties of M-Type Hexagonal $SrFe_{12}O_{19}$ Nanoparticles. *J. Supercond. Novel Magn.* **2015**, *28*, 1589–1599. [CrossRef]
23. Durmus, Z.; Sozeri, H.; Toprak, M.S.; Baykal, A. Effect of Fuel on the Synthesis and Properties of Poly(methyl methacrylate) Modified $SrFe_{12}O_{19}$ Nanoparticles. *J. Supercond. Novel Magn.* **2012**, *25*, 1957–1963. [CrossRef]
24. Roohani, E.; Arabi, H.; Sarhaddi, R.; Sudkhah, S. M-Type Strontium Hexaferrite Nanoparticles Prepared by Sol–gel Auto-combustion Method: The Role of Co Substitution in Structural, Morphological, and Magnetic Properties. *J. Supercond. Novel Magn.* **2017**, *30*, 1599–1608. [CrossRef]

25. Hessien, M.M.; Rashad, M.M.; Hassan, M.S.; El-Barawy, K. Synthesis and magnetic properties of strontium hexaferrite from celestite ore. *J. Alloys Compd.* **2009**, *476*, 373–378. [CrossRef]
26. Xie, T.; Xu, L.; Liu, C.; Ding, S.; Yang, J.; Wu, W. Synthesis and adsorption properties of high specific surface area strontium ferrite from Industrial Strontium Residue. *Vacuum* **2013**, *93*, 71–78. [CrossRef]
27. Liu, B.; Zhang, S.G.; Tian, J.J.; Pan, D.A.; Zhu, H.X. Strontium ferrite powders prepared from oily cold rolling mill sludge by solid-state reaction method. *Rare Met.* **2013**, *32*, 518–523. [CrossRef]
28. Hu, P.; Pan, D.A.; Zhang, S.G.; Tian, J.J.; Volinsky, A.A. Mn-Zn soft magnetic ferrite nanoparticles synthesized from spent alkaline Zn-Mn batteries. *J. Alloys Compd.* **2011**, *509*, 3991–3994. [CrossRef]
29. Winburn, R.S.; Grier, D.G.; Mccarthy, G.J.; Peterson, R.B. Rietveld quantitative X-ray diffraction analysis of NIST fly ash standard reference materials. *Powder Diffr.* **2000**, *15*, 163–172. [CrossRef]
30. Gordani, G.R.; Ghasemi, A.; Saidi, A. Enhanced magnetic properties of substituted Sr-hexaferrite nanoparticles synthesized by co-precipitation method. *Ceram. Int.* **2014**, *40*, 4945–4952. [CrossRef]
31. Chen, W.; Wu, W.W.; Zhou, C.; Zhou, S.F.; Li, M.Y.; Ning, Y. Structural and magnetic properties evolution of Co-Nd substituted M-type hexagonal strontium ferrites synthesized by ball-milling-assisted ceramic process. *J. Electron. Mater.* **2017**, *47*, 2110–2119. [CrossRef]
32. Grewall, J.K.; Kaur, M. Effect of core-shell reversal on the structural, magnetic and adsorptive properties of Fe_2O_3-GO nanocomposites. *Ceram. Int.* **2017**, *43*, 16611–16621. [CrossRef]
33. Loan, T.T.; Nga, T.T.V.; Duong, N.P.; Soontaranon, S.; Hien, T.D. Influence of Structure and Oxidation State on Magnetic Properties of $Sr_{1-x}La_xFe_{12-x}Co_xO_{19}$ Nanoparticles Prepared by Sol–gel Combustion Method. *J. Electron. Mater.* **2017**, *46*, 3396–3405. [CrossRef]
34. Jean, M.; Nachbaur, V.; Bran, J.; Le Breton, J.M. Synthesis and characterization of $SrFe_{12}O_{19}$ powder obtained by hydrothermal process. *J. Alloys Compd.* **2010**, *496*, 306–312. [CrossRef]
35. Wang, Z.; Zhong, L.; Lv, J.; Zheng, H.Q.Y.; Fang, Y.; Jin, M.; Xu, J. Microwave-assisted synthesis of $SrFe_{12}O_{19}$ hexaferrites. *J. Magn. Magn. Mater.* **2010**, *322*, 2782–2785.